A Neural Switch for Active and Passive Fear

Alessandro Gozzi,[1,6,7] Apar Jain,[2,6] Aldo Giovanelli,[3,4] Cristina Bertollini,[3] Valerio Crestan,[1] Adam J. Schwarz,[1] Theodoros Tsetsenis,[2] Davide Ragozzino,[3,5] Cornelius T. Gross,[2,*] and Angelo Bifone[1,7]

[1]Neurosciences CEDD, GlaxoSmithKline Medicines Research Centre, via Fleming 4, 37135 Verona, Italy
[2]Mouse Biology Unit, EMBL, via Ramarini 32, 00015 Monterotondo, Italy
[3]Pasteur Institute–Fondation Cenci Bolognetti and Department of Human Physiology and Pharmacology, Center of Excellence BEMM, University of Rome–La Sapienza, Piazzale Aldo Moro 5, 00185 Roma, Italy
[4]Department of Experimental Medicine, University of L'Aquila, Via Vetoio Coppito 2, 67100 L'Aquila, Italy
[5]Neuromed, Via Atinese 18, 86077 Pozzilli, Italy
[6]These authors contributed equally to this work
[7]Present address: Center for Nanotechnology Innovation, Italian Institute of Technology, IIT@NEST, Pisa, Italy
*Correspondence: gross@embl.it
DOI 10.1016/j.neuron.2010.07.008

SUMMARY

The central nucleus of the amygdala (CeA) serves as a major output of this structure and plays a critical role in the expression of conditioned fear. By combining cell- and tissue-specific pharmacogenetic inhibition with functional magnetic resonance imaging (fMRI), we identified circuits downstream of CeA that control fear expression in mice. Selective inhibition of a subset of neurons in CeA led to decreased conditioned freezing behavior and increased cortical arousal as visualized by fMRI. Correlation analysis of fMRI signals identified functional connectivity between CeA, cholinergic forebrain nuclei, and activated cortical structures, and cortical arousal was blocked by cholinergic antagonists. Importantly, inhibition of these neurons switched behavioral responses to the fear stimulus from passive to active responses. Our findings identify a neural circuit in CeA that biases fear responses toward either passive or active coping strategies.

INTRODUCTION

Research over the past decades has consistently pointed to the amygdala as a key component of the brain's emotional network. Numerous studies in rodents, primates, and humans have demonstrated the involvement of this structure in mediating the emotional, behavioral, and physiological responses associated with fear and anxiety particularly in response to conditioned aversive cues (Aggleton, 1992; Davis and Whalen, 2001; LeDoux, 2000). The amygdala is a highly heterogeneous cluster of forebrain nuclei that can be subdivided into cortical and striatal divisions (Swanson and Petrovich, 1998). The central nucleus (CeA) is located within the striatal division and serves as a major output of the amygdala for the control of mid- and hind-brain circuits involved in physiological and behavioral defensive responses (Amaral et al., 1992). The CeA can be further subdivided into medial and lateral subnuclei whose

neurons express different neuromodulatory receptors (Huber et al., 2005; Tribollet et al., 1988; Veinante and Freund-Mercier, 1997) and appear to differentially project to downstream targets (Jolkkonen et al., 2002). However, it remains unknown how aversive signals are processed within CeA and how this nucleus differentially engages diverse downstream targets to support stimulus-appropriate fear responses.

Using a pharmacogenetic inhibition strategy (Luo et al., 2008) in transgenic mice, we were recently able to show that neural activity in a subset of neurons in CeA is necessary for freezing behavior in response to a conditioned aversive stimulus (Tsetsenis et al., 2007). These neurons, which we called type I cells (Tsetsenis et al., 2007) and which are likely to be similar to type B neurons described in rats (Schiess et al., 1999; Sah et al., 2003; Lopez De Armentia and Sah, 2004), are distinguished from the majority of remaining neurons (called type II, Tsetsenis et al., 2007) by the presence of a prominent depolarizing after-potential. Selective pharmacological suppression of neural activity in type I CeA neurons was achieved by expressing the $G\alpha_i$-coupled serotonin 1A receptor (Htr1a) under the control of a tissue-specific promoter in transgenic mice that are missing the endogenous receptor (the resulting mice are called $Htr1a^{CeA}$). Systemic treatment of $Htr1a^{CeA}$ mice with a selective agonist of Htr1a, 8-hydroxy-2-(di-n-propylamino) tetralin (8-OH-DPAT), led to the opening of G protein coupled inward rectifying potassium (GIRK) channels, membrane hyperpolarization, and suppression of neural firing (Tsetsenis et al., 2007). A suppression of conditioned freezing behavior following inhibition of CeA neurons is consistent with the proposed role of CeA as an output circuit that promotes autonomic and behavioral responses to conditioned fear (Wilensky et al., 2006). Here, we combine pharmacogenetic inhibition of neural activity in CeA with functional magnetic resonance imaging (fMRI) to map in vivo neural activity in circuits downstream of CeA that are involved in conditioned fear responding. This approach identified ventral forebrain cholinergic neurons as a critical downstream target of CeA and demonstrated that type I cells within CeA actively suppress cholinergic-mediated cortical arousal and exploratory behavior at the same time as promoting freezing responses and thus serve as a switch between active and passive fear.
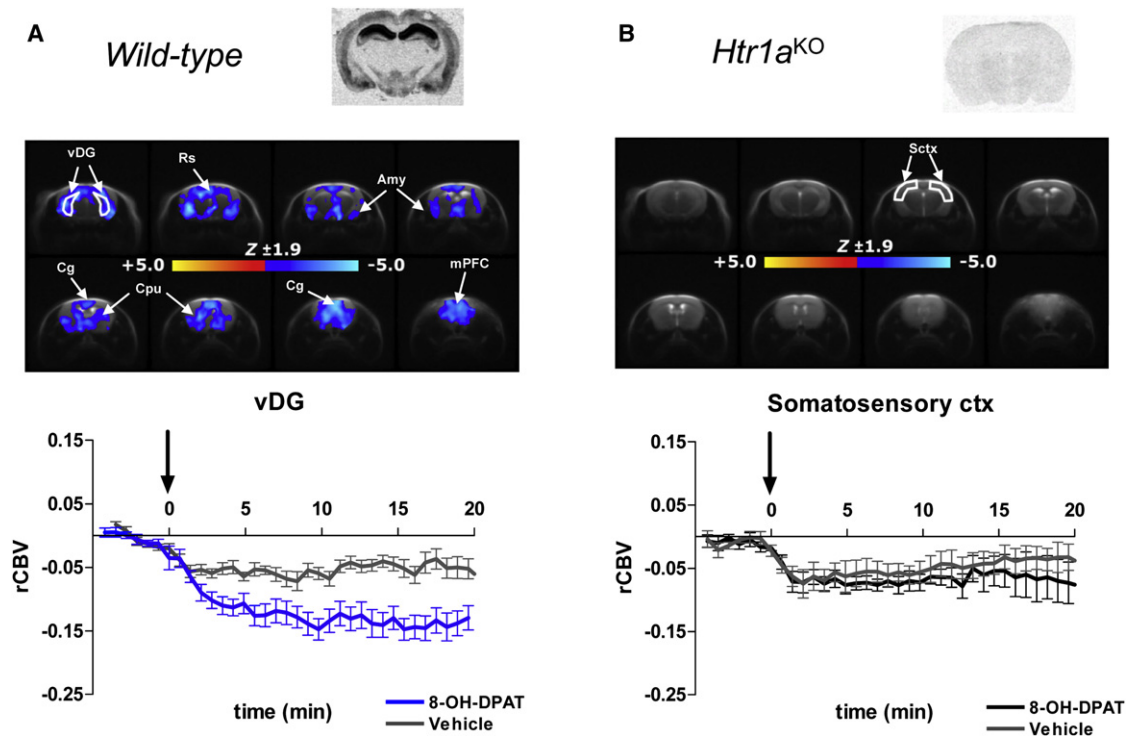
Figure 1. Pharmacological Activation of Htr1a Leads to Widespread Inhibition of Neural Activity in Wild-Type Mice

Anatomical distribution of the rCBV changes produced by administration of the Htr1a agonist, 8-OH-DPAT (0.5 mg/kg i.a.) in (A) wild-type (n = 14) and (B) Htr1a knockout (Htr1a^KO, n = 8) mice. Blue indicates significantly *reduced* rCBV compared with vehicle baseline (Z > 1.96, cluster correction, p = 0.01). For each mouse line the rCBV time course following vehicle or 8-OH-DPAT injection in a representative brain region is shown below each map (vDG, ventral dentate gyrus; Rs, retrosplenial cortex; Amy, amygdala; Cg, cingulate cortex; Cpu, caudate putamen; mPFC, medial prefrontal cortex; Sctx, somatosensory cortex). A significant decrease in rCBV was observed following 8-OH-DPAT treatment in wild-type, but not Htr1a^KO mice, demonstrating the feasibility of using rCBV to map Htr1a-dependent inhibition of neural activity. Htr1a receptor distribution (^{125}I-MPPI autoradiography) in a representative brain slice for each strain is shown for reference.

RESULTS

fMRI Mapping of Neural Activity Following Cell-Type-Specific Inhibition

To determine the feasibility of using fMRI to map neural activity changes following cell type-specific neural inhibition using the Htr1a-based system (Tsetsenis et al., 2007), wild-type mice were placed in the MR scanner and fMRI signal changes induced by systemic administration of the Htr1a agonist 8-OH-DPAT (0.5 mg/kg i.a.) were examined. For all studies, we used relative cerebral blood volume (rCBV) as a surrogate for the underlying changes in neural activity (Sheth et al., 2004). This measure has gained acceptance as the measure of choice in small animal fMRI studies where sensitivity is a significant technical challenge (Chen et al., 2001; Jenkins et al., 2003). Consistent with the efficient coupling of Htr1a to inhibitory GIRK channels (Luscher et al., 1997), systemic treatment with 8-OH-DPAT led to a significant and widespread decrease in rCBV in all structures where Htr1a is expressed (Figure 1A), including striatum, amygdala, ventral hippocampus, and prefrontal, cingulate, insular, and rhinal cortices (Z > 1.96, cluster corrected at p = 0.05). The time profile of the effect was similar in all regions examined, with a sustained negative response that lasted throughout the time-window examined (Figure S1). As seen previously (Gozzi

et al., 2007; Schwarz et al., 2006), vehicle injection produced a small decrease in rCBV that probably reflected dilution of the blood-pool contrast agent.

Importantly, the agonist-induced decrease in rCBV was absent in Htr1a knockout mice confirming the selectivity of 8-OH-DPAT for Htr1a at this dose in vivo (Figure 1B). As expected, time profiles of rCBV following vehicle or 8-OH-DPAT administration in knockout mice (Htr1a^KO) showed substantial overlap in all regions examined (Figure S1). Similarly, image-based analysis did not highlight significant agonist-induced activation or deactivation (Z > 1.96, cluster correction p = 0.05). These data indicate that neural inhibition associated with activation of Htr1a can be mapped in vivo using pharmacological fMRI.

Suppression of Type I CeA Neurons Leads to Widespread Cortical Activation

Next, we examined rCBV changes following agonist-induced inhibition of type I neurons in CeA using Htr1a^CeA mice (Htr1a^KO/Htr1a^KO;Nrip2-Htr1a/+; Tsetsenis et al., 2007). Unexpectedly, a significantly increased rCBV signal was seen in several forebrain areas, including cerebral cortex, thalamus, ventral hippocampus, amygdala, caudate putamen, and septum (Figure 2). Time course analyses of the rCBV response to
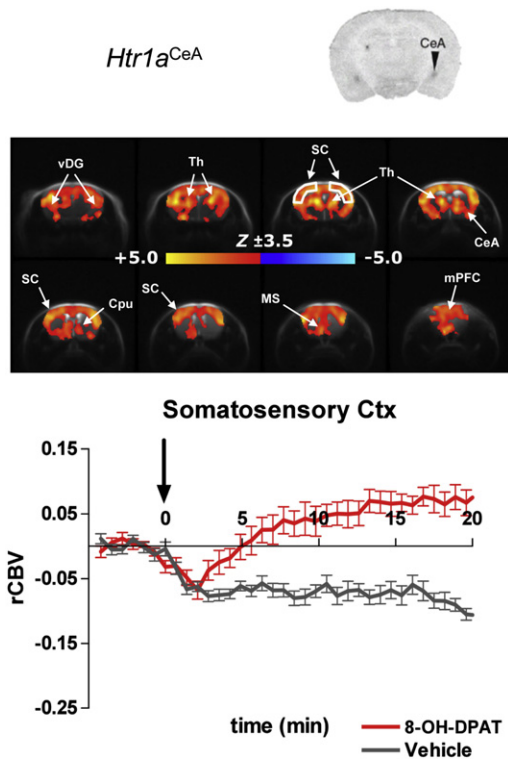
Figure 2. Cortical Arousal Following Suppression of Type I CeA Cells

Neural activity as measured by rCBV using fMRI in *Htr1a*^CeA mice treated with the Htr1a agonist, 8-OH-DPAT (0.5 mg/kg i.a., n = 9). Yellow/orange indicates significantly *increased* rCBV compared with vehicle baseline (Z > 3.5; cluster correction p = 0.01). Bottom panel shows rCBV time course following vehicle or 8-OH-DPAT injection in the somatosensory cortex. Significant increases in rCBV were detected following agonist treatment in several regions, including cerebral cortex, thalamus, ventral hippocampus, amygdala, caudate putamen, and septum. Htr1a receptor distribution (^125I-MPPI autoradiography) in a representative brain slice of *Htr1a*^CeA is reported for reference (vDG, ventral dentate gyrus; Th, thalamus; Cpu, caudate putamen; mPFC, medial prefrontal cortex; SC, somatosensory cortex; MS, medial septum).

8-OH-DPAT in representative regions of interest (ROIs) revealed a sustained activation that lasted throughout the time-window examined (Figure S2). Again, no agonist-induced activation was seen in knockout littermates (*Htr1a*^KO; Figure 1B; Figure S1).

In order to map neural circuits that mediate cortical activation in *Htr1a*^CeA mice following agonist treatment, we applied correlation analysis to the regional fMRI responses. This approach aims to elucidate relationships between signals elicited by agonist challenge in spatially distinct brain regions and complements the univariate approach applied to generate rCBV maps (Figures 1 and 2). These correlations can be interpreted as reflecting functional connectivity between the regions involved (Schwarz et al., 2007a) and can be used to resolve specific brain circuits engaged by pharmacological agents (Schwarz et al., 2007b). Correlation analysis revealed brain regions whose agonist-induced rCBV responses significantly correlated with a seed region located in CeA (Figure 3A). A significant pattern of correlated activity was identified linking CeA with cholinergic nuclei in the ventral forebrain, including substantia innominata

(SI), diagonal band (DB), and nucleus basalis of Meynert (NBM) in 8-OH-DPAT-treated *Htr1a*^CeA mice (Figure 3A). A similar analysis of bottom-up connectivity from the cortical regions most strongly activated by 8-OH-DPAT in the same group showed significant connectivity between cortex and the same cholinergic nuclei (SI, DB, and NBM; Figure 3B). This connectivity is consistent with anatomical and functional studies demonstrating cholinergic innervation of cortex by these structures in rodents (Mesulam et al., 1983). When considered together with the findings of our univariate analysis (Figure 2), these results suggest that suppression of neural activity in type I CeA neurons leads to a disinhibition of selected ventral forebrain cholinergic nuclei and a consequent arousal of cortical circuits.

To test the hypothesis of a functional involvement of cholinergic circuits in the observed cortical arousal, we performed fMRI mapping in response to 8-OH-DPAT in *Htr1a*^CeA mice pretreated with atropine, an antagonist of muscarinic acetylcholine receptors. Atropine-sulfate (0.3 mg/kg, i.p.) significantly attenuated 8-OH-DPAT induced activation in all brain regions examined (Figures 3C and S3). Importantly, atropine-methylnitrate (0.3 mg/kg, i.p.), an atropine salt with poor blood-brain barrier penetration (Boccia et al., 2003), did not significantly block cortical arousal (Figures 3D, S2, and S3) arguing against a role of peripheral cholinergic receptors in mediating the effect. Moreover, atropine sulfate did not attenuate the rCBV response to 8-OH-DPAT in wild-type mice (Figure S3). These findings support a role for central cholinergic disinhibition in the cortical arousal seen after silencing of type I CeA neurons and are consistent with our functional connectivity mapping analysis.

Switch from Passive to Active Conditioned Behavior

Next, we examined the behavioral correlates of cortical arousal following suppression of type I CeA neuron activity. As previously reported (Tsetsenis et al., 2007), *Htr1a*^CeA mice treated with 8-OH-DPAT (0.2 mg/kg, s.c.) showed a significant reduction of freezing behavior during the tone when compared with vehicle-treated *Htr1a*^CeA mice (Figure 4A) and no change in freezing to the tone was seen in agonist-treated *Htr1a*^KO control littermates (ANOVA – genotype × treatment effect for freezing to the tone: $F[1, 100] = 4.51$, p = 0.0362, n = 19-30; Figure 4B). However, agonist-treated *Htr1a*^CeA mice also showed a significant increase in several exploratory and risk assessment behaviors, including digging, *exploration*, and rearing (Figure 4C). When summed as total active behavior (cumulative digging, *exploration*, and rearing), agonist-treated *Htr1a*^CeA, but not *Htr1a*^KO mice showed a dramatic shift from passive to active conditioned behavior during the tone (ANOVA – genotype × treatment effect on active behavior during tone: $F[1,100] = 4.475$, p = 0.0369, n = 19-30; Figures 4A–4D). Notably, agonist treatment produced only a small, nonsignificant increase in active behaviors in *Htr1a*^CeA mice during the prestimulus period and a similar trend was seen in *Htr1a*^KO mice (data not shown). These data argue for a shift in the quality of responses to the conditioned aversive stimulus following inhibition of type I CeA neurons. To determine whether active and passive behaviors were mutually exclusive expressions of fear, we examined within-animal correlations of active and passive behavior during exposure to the conditioned stimulus. An inverse correlation
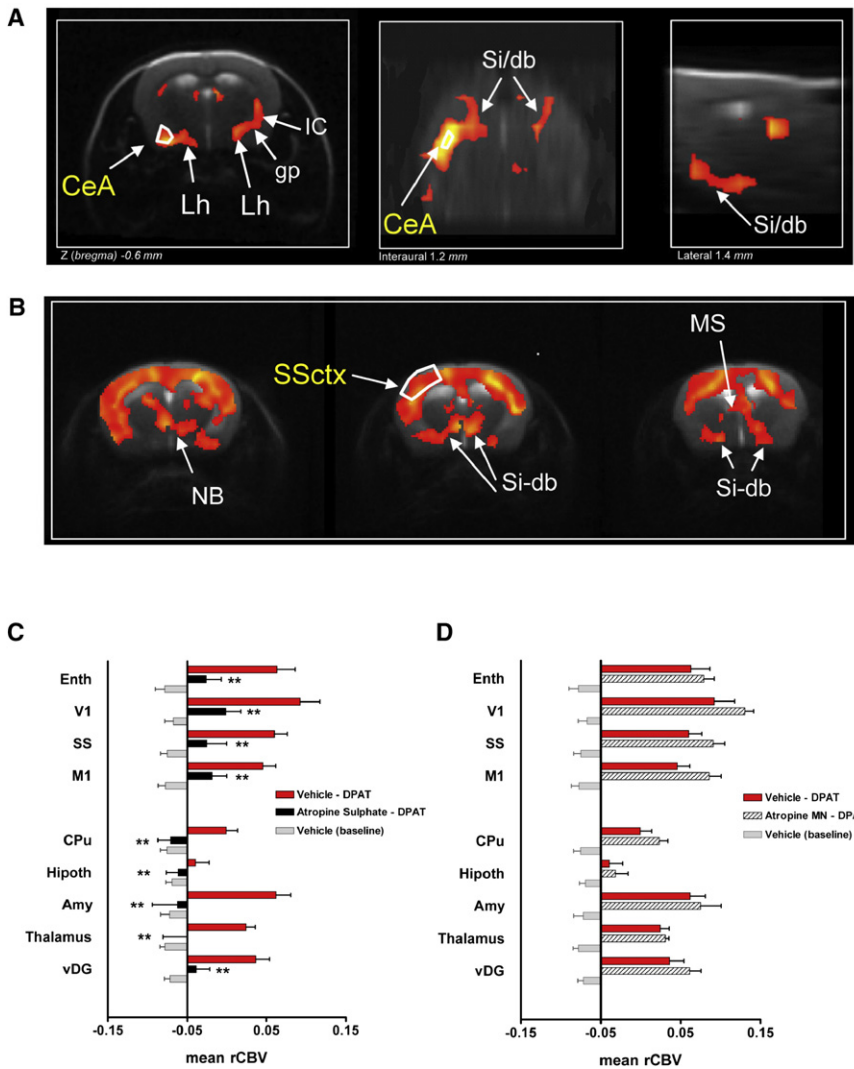
Figure 3. Atropine Blocks Cortical Arousal Following Inhibition of Type I CeA Cells

Maps of 8-OH-DPAT-induced rCBV response that significantly correlated with rCBV signal in (A) CeA and (B) somatosensory cortex (SSctx) in $Htr1a^{CeA}$ mice (Z > 1.6, cluster correction p = 0.01, n = 9). The three images in (A) refer to three perpendicular sections located at Z_{bregma} −0.6 mm, interaural 1.2 mm, and lateral 1.4 mm, respectively. Significantly correlated rCBV signal was detected between CeA, Si, and db and between SSctx, Si, db, MS, and NB, suggesting a functional connectivity network linking CeA, ventral forebrain cholinergic nuclei, and neocortex. Pretreatment with (C) atropine sulfate (n = 5), but not (D) a non-brain penetrant salt of atropine (atropine methyl-nitrite, n = 5) blocked the rCBV signal increases seen after 8-OH-DPAT (0.5 mg/kg i.a) treatment of $Htr1a^{CeA}$ mice (n = 9; **p < 0.01 versus vehicle-pretreated subjects, one-way ANOVA followed by Fisher's LSD test; CeA, central nucleus of the amygdala; LH, lateral hypothalamus; gp, external globus pallidus; IC, internal capsule; Si, substantia inno-minata; db, nucleus of the diagonal band of Broca; MS, medial septum; NB, nucleus basalis of Meynert; SS, somatosensory cortex; M1, motor cortex; Hipoth, hypothalamus; Amy, amygdala; CPu, caudate putamen; V1, visual cortex; Enth, entorhinal cortex).

effect on freezing and/or active behaviors during the tone in agonist-treated $Htr1a^{KO}$ mice suggesting normal fear recall in the presence of atropine (Figures 4F and 4H). In $Htr1a^{CeA}$ mice, however, atropine pretreatment significantly reversed the suppression of freezing behavior and showed a trend for a reversal of the induction of active behaviors following 8-OH-DPAT treatment (Figures 4E and 4G). These data suggest that cholinergic neurotransmission directly contributes to the switch between passive and active behavioral responses. Notably, however, the low dose of atropine (0.1 mg/kg) had a significant and selective effect on freezing, while leaving active behaviors unaltered (Figures 4E and 4G). This dissociation reveals that active and passive behaviors are differentially dependent on cholinergic neurotransmission.

Activation of Oxytocin-Responsive Neurons in Lateral CeA

Given the dissociation between oxytocin and vasopressin receptor-expressing GABAergic projection neurons in lateral and medial CeA, respectively (Veinante and Freund-Mercier, 1997) and the exclusive enervation of SI/NBM by lateral, but not medial CeA projections (Jolkkonen et al., 2002), we considered whether type I cells might selectively inhibit oxytocin receptor-expressing cells in the lateral CeA. Whole-cell recordings in lateral CeA neurons in slices from $Htr1a^{CeA}$ and $Htr1a^{KO}$ littermates confirmed the presence of depolarizing
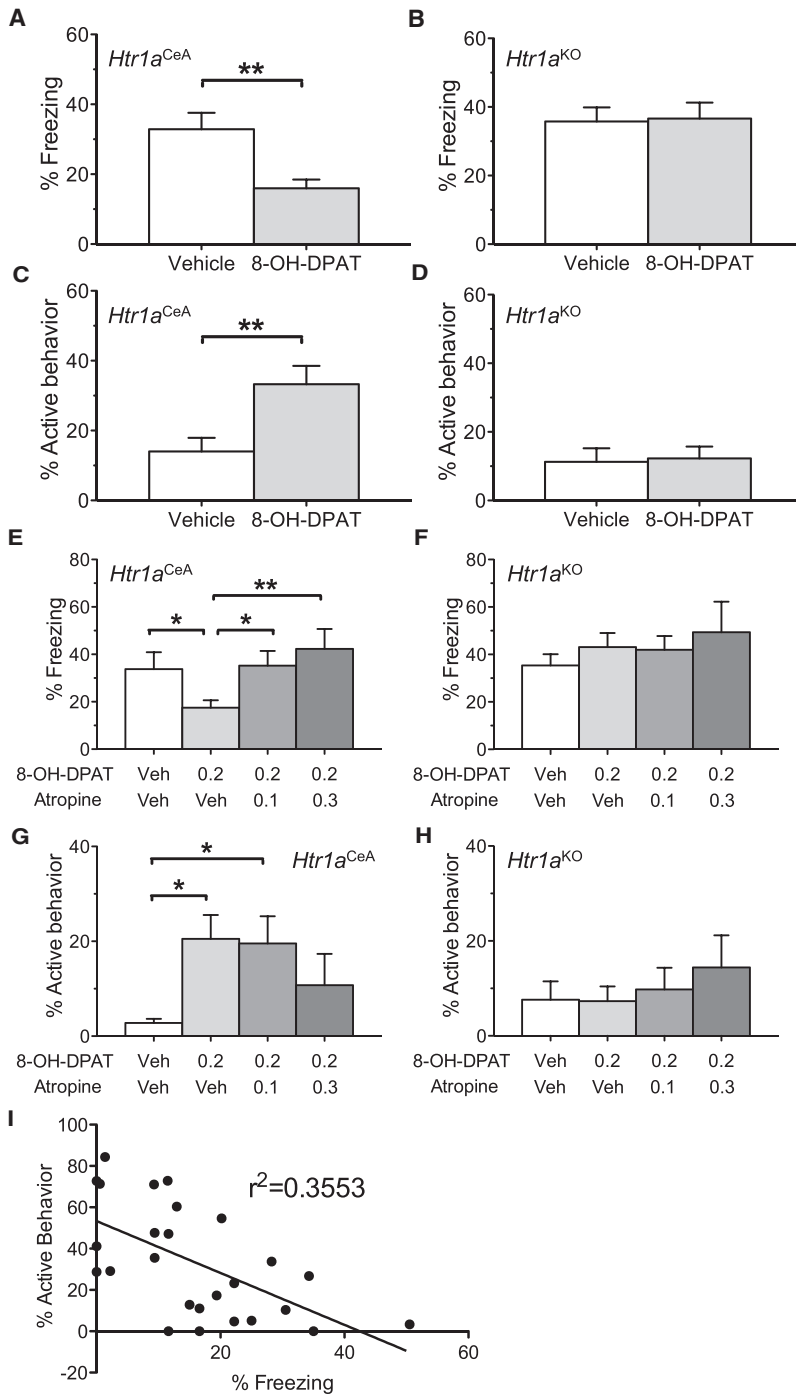
emerged between freezing and active behavior (r^2 = 0.35; Figure 4I), suggesting that expression of these responses was codependent.

One interpretation of our findings is that suppression of type I CeA neurons induced cortical arousal during behavioral testing, and this cortical activity directly contributed to a shift in behavioral responses to the conditioned stimulus. First, we tested whether inhibition of type I cells was associated with cortical arousal in awake behaving mice by performing c-Fos immunohistochemistry following treatment of $Htr1a^{CeA}$ and $Htr1a^{KO}$ littermates with 8-OH-DPAT (0.2 mg/kg, s.c.). The number of c-Fos-positive cells in the anterior cingulate area (a region showing prominent rCBV increases following agonist treatment; Figure 2) was significantly greater in agonist-treated $Htr1a^{CeA}$ than $Htr1a^{KO}$ mice (Figure 5). These findings confirmed increased cortical neuron activity following suppression of type I CeA neurons in behaving mice. Second, we examined whether pretreatment with atropine was able to interfere with behavioral responses to the fear stimulus. While atropine had no significant

Figure 4. Switch from Passive to Active Fear Responses Following Inhibition of Type I CeA Cells

Behavioral analysis of $Htr1a^{CeA}$ and $Htr1a^{KO}$ mice pretreated with either vehicle (saline, s.c.) or the Htr1a agonist, 8-OH-DPAT (0.2 mg/kg, s.c.) during exposure to a tone (3 min) previously associated with footshock revealed a reduction in duration of freezing and increase in duration of active exploratory/risk assessment behavior in (A and C) $Htr1a^{CeA}$ (vehicle: n = 19, agonist: n = 26), but not (B and D) $Htr1a^{KO}$ mice (vehicle: n = 29, agonist: n = 30). Active behavior was scored as cumulative digging, exploration, and rearing. Atropine pretreatment (0.1 and 0.3 mg/kg, i.p.) caused a significant reversal of the inhibition of freezing seen following 8-OH-DPAT-treatment in (E) $Htr1a^{CeA}$ (vehicle: n = 10, 8-OH-DPAT: n = 17, low atropine: n = 19, high atropine: N = 9), but not (F) $Htr1a^{KO}$ mice (vehicle: n = 20, 8-OH-DPAT: n = 20, low atropine: n = 17, high atropine: n = 7), while showing a trend for a reversal of the increase in active behavior seen following 8-OH-DPAT-treatment at the higher dose in (G) $Htr1a^{CeA}$, but not (H) $Htr1a^{KO}$ mice. (I) Plot of active behavior against freezing in individual $Htr1a^{CeA}$ mice treated with 8-OH-DPAT (n = 26) revealed a negative correlation (r^2 = 0.355, p = 0.0013) between active and passive fear responses (*p < 0.05, **p < 0.01).

effect on firing of type I cells (Figures 6D–6E), but significantly increased firing of type II cells (Figures 6I–6J) consistent with the selective expression of oxytocin receptor on this class of cells. Importantly, type II cells also showed excitatory responses to 8-OH-DPAT (Figures 6G and 6H), while the Htr1a agonist had no significant effect on firing of this class of neuron in slices from $Htr1a^{KO}$ controls (1.07 ± 0.19 to 1.00 ± 0.22 Hz; n = 3, p = 0.3). Oxytocin receptor-expressing cells in lateral CeA are known to inhibit vasopressin receptor-expressing cells in medial CeA (Huber et al., 2005), and recordings from the medial subnucleus in our preparations confirmed inhibitory effects of TGOT (data not shown). Together, these data are consistent with type I CeA neurons being local inhibitory neurons that tonically suppress firing of oxytocin receptor-expressing type II projection neurons in lateral CeA.

DISCUSSION

We have used pharmacological fMRI to map circuits downstream of the amygdala that are involved in the expression of conditioned fear responses. Our findings point to ventral forebrain cholinergic nuclei as a critical downstream target of CeA that promote cortical arousal and facilitate active responses at the expense of passive responses to a conditioned aversive stimulus. Several conclusions can be drawn from our study in light of previous anatomical and functional studies. First, anterograde tracing studies demonstrate that projections from amygdala to ventral forebrain cholinergic

after-potential (DAP) positive, type I (Figure 6A) and DAP-negative, type II (Figure 6F) neurons in this subnucleus (Tsetsenis et al., 2007). Application of 8-OH-DPAT (50 μM, 1–3 min) caused inhibition of cell firing in type I neurons of $Htr1a^{CeA}$ (Figures 6B and 6C), but not $Htr1a^{KO}$ (3.51 ± 0.88 Hz to 3.05 ± 0.99 Hz; n = 7, p = 0.13) mice, consistent with our previous observations (Tsetsenis et al., 2007). Application of the oxytocin receptor agonist [Thr[4], Gly[7]]-oxytocin (TGOT, 0.2 μM, 1–3 min) had no
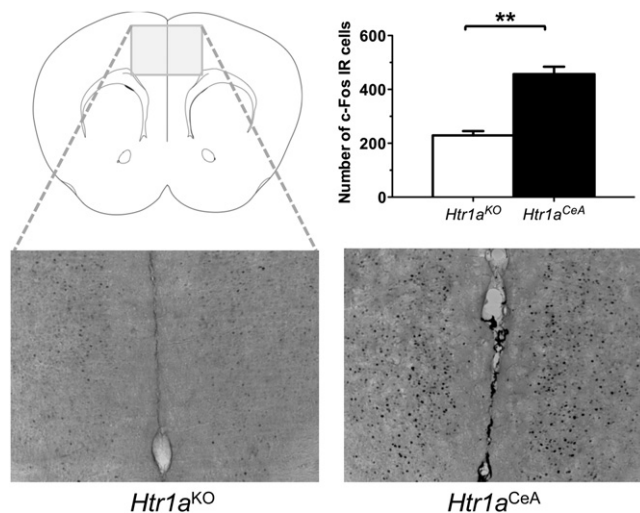
Figure 5. Increased Cortical c-Fos Immunoreactivity Following Inhibition of Type I CeA Cells

Quantification of c-Fos immunoreactivity in sections from brains of mice 90 min after treatment with 8-OH-DPAT (0.2 mg/kg, s.c.). A significantly greater increase in the number of c-Fos IR-positive nuclei was seen in the anterior cingulate area (ACA) of $Htr1a^{CeA}$ (n = 4) versus $Htr1a^{KO}$ (n = 3) mice (**p < 0.001).

nuclei such as SI, DB, and NBM originate exclusively from the lateral and/or capsular subnuclei of CeA (Jolkkonen et al., 2002). Because these connections make symmetric synapses onto neurons in the vicinity of cholinergic cell bodies in these target nuclei, they are likely to be GABAergic projection neurons that regulate activity of cholinergic neurons via inhibition of local GABAergic interneurons (Jolkkonen et al., 2002). An excitatory role for CeA on cortical activity is confirmed by electrophysiological studies that demonstrate a shift from large irregular slow activity (synchronous) to low voltage fast (asynchronous) cortical activity following electrical stimulation of CeA, an effect that is blocked by the cholinergic antagonist scopolamine (Dringenberg and Vanderwolf, 1997). Our electrophysiological studies demonstrate that type II cells are likely to be identical to the GABAergic, oxytocin receptor-expressing projection neurons previously described in the lateral CeA (Huber et al., 2005). Firing of these cells was consistently increased by bath application of the Htr1a agonist in $Htr1a^{CeA}$ mice (Figures 6G and 6H), consistent with a direct inhibitory connection between type I and type II cells in lateral CeA. Thus, we speculate that type II neurons in lateral CeA are equal to the previously described CeA-SI/NBM projecting neurons (Jolkkonen et al., 2002) and are responsible for mediating the cortical arousal seen in our fMRI (Figure 2) and c-Fos (Figure 5) mapping studies.

Second, previous work has shown that oxytocin receptor-expressing cells in lateral CeA also project to and directly inhibit vasopressin receptor-expressing cells in medial CeA (Huber et al., 2005; data not shown). Efferents from the medial CeA project to hypothalamic and brainstem circuits that control freezing and autonomic fear responses and are thought to be responsible for conditioned freezing and autonomic responses to painful stimuli (Ehrlich et al., 2009). Thus, it is possible that

disinhibition of type II cells by Htr1a agonist treatment in $Htr1a^{CeA}$ mice suppresses conditioned freezing in part by directly inhibiting medial CeA projection neurons.

Third, our experiments showing that atropine blocked the switch from freezing to active behavior suggest that ventral forebrain cholinergic circuits are critical for modulating the quality of fear responses. Whether this switch is a direct consequence of increased cortical arousal or is also in part due to increased inhibition of medial CeA outputs that have been proposed to be responsible for behavioral immobility is not completely clear from our results. Our observation that atropine was able to completely reverse the effects of 8-OH-DPAT at least on freezing suggest that cholinergic mechanisms are necessary (but not necessarily sufficient) to switch away from passive fear (Figure 4E). The apparent reduced efficacy of atropine in reversing active behaviors induced by the Htr1a agonist (Figure 4G) suggests either that these are less sensitive to atropine or that other circuits are involved.

Thus, our data suggest a model in which the activity of lateral CeA projection neurons determines CeA outputs, switching behavioral responses from freezing to risk assessment and exploration (Figure 7). Under normal conditions (switch ON), lateral CeA projection neurons are tonically inhibited by type I neurons and medial CeA projection neurons are free to respond to inputs and promote freezing. When type I neurons are silenced (switch OFF) type II, oxytocin receptor-expressing lateral CeA projection neurons are disinhibited, leading to increased lateral CeA outputs to ventral forebrain and inhibition of medial CeA outputs. CeA efferents to the ventral forebrain (NBM/SI) lead to a disinhibition of cholinergic neurons and increased cortical arousal. Blockade of cholinergic neurotransmission is able to reverse the behavioral effects of the switch, suggesting that CeA-ventral forebrain outputs play a critical role in the switch. Such a circuitry is consistent with the suppression and facilitation of fear responses reported after intra-CeA administration of oxytocin and vasopressin receptor agonists, respectively (Roozendaal et al., 1992) and is in agreement with existing models of CeA function (Viviani and Stoop, 2008; Walker and Davis, 2008; Ehrlich et al., 2009).

One possible confound in the interpretation of our fMRI results is the possibility that low levels of expression of Htr1a outside type I CeA neurons may have contributed to the signal observed. Several lines of evidence suggest that such ectopic activation, if present, is minimal and does not mediate the rCBV and behavioral effects seen following 8-OH-DPAT treatment. First, similar experiments in a line of mice expressing Htr1a under the same promoter but showing expression selectively in dentate gyrus granule cells of the hippocampus ($Htr1a^{DG}$; Tsetsenis et al., 2007) did not show any increase in cortical rCBV signal (Figure S4) despite the fact that this line shows low levels of Htr1a expression in CeA (Tsetsenis et al., 2007). Thus, low levels of Htr1a do not appear to cause membrane hyperpolarization sufficient to alter neuronal firing, and this conclusion is confirmed by electrophysiological studies in slices taken from these mice (Tsetsenis et al., 2007). Second, the ability of centrally delivered atropine to suppress rCBV signal activation following 8-OH-DPAT treatment argues against the effect being mediated by activation of Htr1a within a local cortical circuit. Another possible
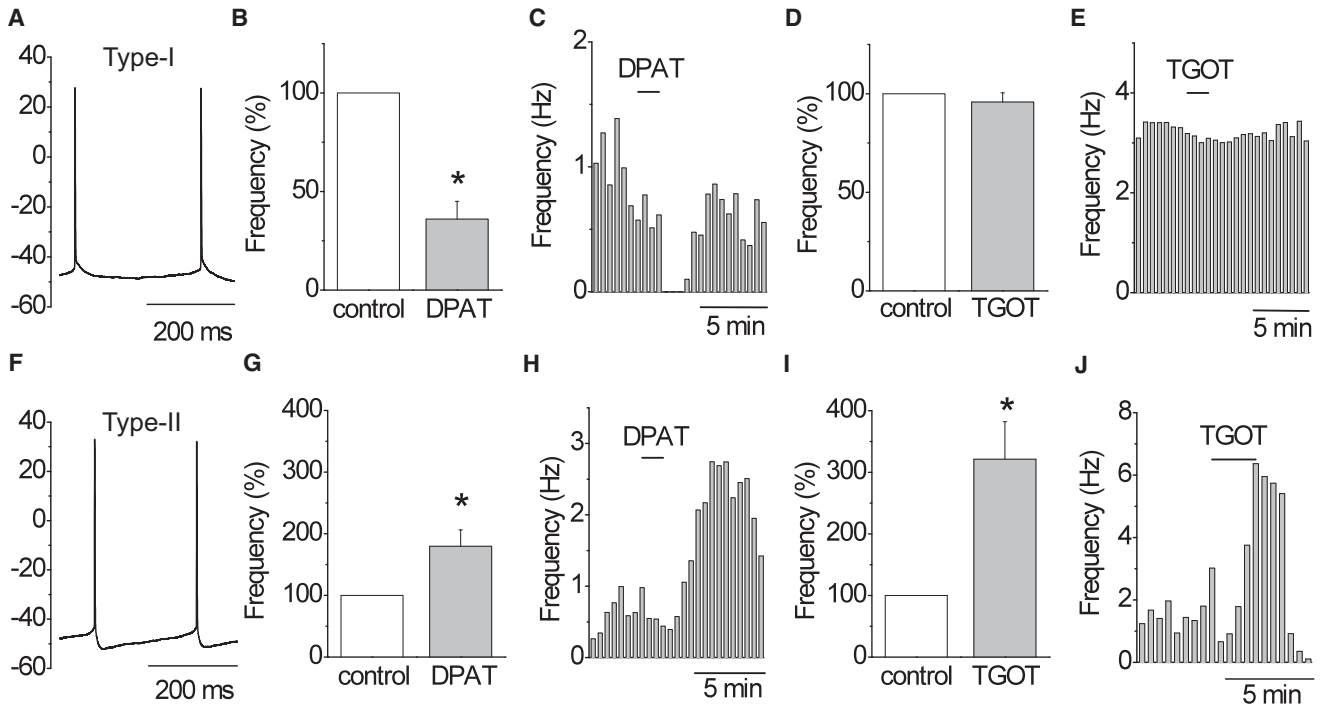
Figure 6. Type I CeA Cells Tonically Suppress Firing of Oxytocin-Responsive Neurons in Lateral CeA
Distinct firing signatures distinguished two major cell types in lateral CeA: (A) DAP[+] type I and (F) DAP[−] type II neurons. Whole-cell recordings in lateral CeA neurons of slices taken from $Htr1a^{CeA}$ mice demonstrated that bath application of 8-OH-DPAT (DPAT, 50 μM, 1–3 min) induced a significant decrease in spontaneous firing of type I cells (B and C, n = 7) and increase in firing of type II cells (G and H, n = 9). Type II cells (I–J, n = 7), but not type I cells (D and E, n = 5) showed increased firing following application of the oxytocin receptor agonist, [Thr[4], Gly[7]]-oxytocin (TGOT, 0.2 μM, 1–3 min). (B, D, G, and I) Relative mean firing frequency expressed as percentage of control value before drug delivery. (C, E, H, and J) Time course of the firing frequency of a representative cell. No significant changes in neuronal firing following 8-OH-DPAT administration were seen in slices taken from $Htr1a^{KO}$ control mice (type I cells: 3.51 ± 0.88 to 3.05 ± 0.99 Hz, n = 7, p = 0.13).

confound derives from or use of a Htr1a knockout background for our studies. While these mice do show significant behavioral and physiological differences these are unlikely to have affected our conclusions given the combination of pharmacological (8-OH-DPAT versus vehicle) and genetic ($Htr1a^{CeA}$ versus $Htr1a^{KO}$) controls.

An important question raised by our findings is whether type I CeA neurons are selectively involved in phasic, conditioned fear responses (Walker and Davis, 2008), or whether they also actively modulate tonic, unconditioned behavior. The fact that we detected cortical arousal following agonist treatment in both unstimulated, anaesthetized and awake, freely moving animals suggests that type I CeA neurons are tonically active in the absence of any conditioned stimulus. However, active behaviors, although in some cases present before stimulus presentation, were significantly enhanced only during the tone
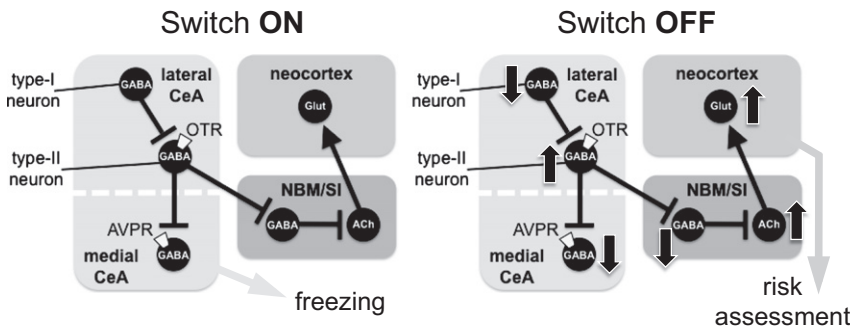

Figure 7. Proposed Circuit by which CeA Influences Active and Passive Fear Responses
Under standard conditions (Switch ON) type I cells are responsible for tonically inhibiting type II oxytocin receptor-expressing neurons in lateral CeA that project to nucleus basalis of Meynert and substantia innominata (NBM/SI). When type I cells are inhibited (Switch OFF), oxytocin receptor-expressing GABAergic projection neurons in lateral CeA are disinhibited. Increased firing of lateral CeA projection neurons leads to inhibition of ventral forebrain interneurons that maintain suppression of firing of cholinergic neurons responsible for promoting neocortical arousal. Blocking cholinergic neocortical activation (e.g., with the muscarinic antagonist atropine) leads to a reversal of the switch from passive to active behavior. Oxytocin receptor-expressing lateral CeA neurons also directly inhibit vasopressin receptor-expressing medial CeA neurons that project to hypothalamic and brainstem structures to promote freezing and parasympathetic responses to aversive conditioned stimuli (OTR, oxytocin receptor; AVPR, arginine/vasopressin receptor; arrows highlighted in white indicate relative changes in neuronal firing).

(data not shown) suggesting that relief of tonic inhibition in CeA was not sufficient to moderate behaviors in the absence of appropriate upstream inputs. Thus, we conclude that CeA disinhibition permits the expression of exploratory and risk assessment behaviors in the presence of a fear stimulus, but that this disinhibition is not sufficient to modulate unconditioned fear responses that may converge at a lower level in the fear circuitry.

Another question of importance is whether the switch from passive to active behavior we see reflects a change in the quality of the fear response or rather a change in its intensity. Although our observed behavioral switch is clearly one of quality, rather than quantity, it is possible that it acts to regulate the activity of a single downstream circuit. Lesions of the dorsal premamillary nucleus, for example, can transform fear in the presence of a predator from freezing to cautious exploration, and, contextual fear of the predator from cautious to relaxed exploration (Cezario et al., 2008), for example. Thus, the CeA switch may be acting on a downstream rheostat-like circuit that dials between freezing/risk assessment/nonfear in a way that is consistent with the defensive distance hypothesis. Alternatively, the CeA switch could be acting independently to suppress passive and promote active behaviors. Our observation that low doses of atropine (0.1 mg/kg) selectively reverses the effects of 8-OH-DPAT on freezing in $Htr1a^{CeA}$ mice, while leaving active behaviors unaffected (Figures 4G and 4H), suggests that separate circuits may be involved in these two coping strategies. A related question involves the degree to which variation in CeA switch efficacy might explain individual variation in fear behavior. It is possible, for example, that different set points of tonic activity of type I CeA cells could predispose animals to a more passive or active fear coping style. Future experiments aimed at examining the role of defensive distance or intensity as well as interindividual variability in modulating the CeA switch may help in address these hypotheses.

In summary, we have applied fMRI and correlation analysis to map circuits downstream of CeA that are involved in modulating conditioned fear. Our findings demonstrate that CeA outputs to ventral forebrain cholinergic neurons driving cortical arousal are under tonic inhibition by type I neurons in CeA and that modulation of their activity offers the animal a route to shift its conditioned fear responses from passive to active behaviors. These findings demonstrate that CeA circuits are involved in determining both the magnitude and quality of conditioned fear responses and is consistent with studies arguing in favor of a more complex role for the amygdala in modulating fear coping behavior (Walker and Davis, 2008;Wilensky et al., 2006).

EXPERIMENTAL PROCEDURES

Animals
All in vivo studies were conducted in accordance with the laws of the Italian Ministry of Health (DL 116, 1992). Protocols were reviewed and approved by a local animal care committee in accordance with the guidelines of the Principles of Laboratory Animal Care (NIH publication 86-23, revised 1985). fMRI experiments were performed in adult (>10 weeks) male mice. The transgenic lines used have been previously described (Tsetsenis et al., 2007). The strains were maintained on a mixed C57BL/6J;CBA/J;129S6/SvEvTac background. Littermates were used for all control experiments. Experiments on the effect of atropine sulfate on the inhibitory action of 8-OH-DPAT in wild-

type mice were performed in C57BL/6J male mice (Charles River Italia, Como, Italy). Animals used in fMRI studies were singly housed with food and water provided ad libitum and under controlled temperature (20°C–22°C), humidity (45%–65%), and lighting (12 hr light/dark, lights on at 06:00 hr). Animals used in behavioral studies were housed as previously described (Tsetsenis et al., 2007).

Animal Anesthesia and Physiological Monitoring
Mice were anaesthetized with 4% isoflurane in a 1:1 oxygen/nitrogen mixture (0.9 l/min + 0.9 l/min) within an induction chamber connected to a vaporizer (Burtons Medical Equipment, UK). The animal was then placed supine on an interactive heating pad (Harvard Apparatus, UK) and gaseous anesthesia continuously delivered through a face mask. Mice were subsequently tracheotomized and artificially ventilated (see below). The left femoral artery was cannulated for compound administration, continuous blood pressure monitoring, infusion of paralyzing agent (pancuronium bromide, 0.5 mg/kg/hr, Sigma-Aldrich, Italy), and blood sampling for measurement of arterial blood gases. $Htr1a^{CeA}$ and wild-type animals were also fitted with an intraperitoneal cannula to allow administration of anticholinergic drugs. Arterial blood gases p_aCO_2 and p_aO_2 were measured terminally and the values used retrospectively to exclude subjects that presented parameters outside the physiological range (20–50 mmHg for p_aCO_2, > 80 mmHg for p_aO_2). Mean weight and p_aCO_2 levels recorded are reported in Supplemental Information (Table S1). No statistically significant difference in postacquisition p_aCO_2 values between any of the groups was observed (one-way ANOVA followed by Fisher's LSD and Hochberg's correction for multiple comparisons with $\alpha = 0.05$).

Tracheostomy
Prior to surgical incision, each mouse received a subcutaneous infiltration of 0.05% tetracaine solution at each surgical site (neck and femoral area) at volume of 0.02 ml/point (0.04 ml/mouse). Tetracaine was chosen due to its negligible degree of brain penetration (Ferrari et al., 2010). The neck and femoral area were shaved with an electrical shaver and the skin disinfected. Rolled gauze was placed under the neck in order to extend it and facilitate the subsequent exposure of trachea for surgery incision. A midline skin incision was made along the length of the neck and, after separating the two halves of the sternohyoid muscle, the trachea exposed. The incision covered the sublaryngeal region, and a G23 cannula (Vygon, France), shortened to 0.7 cm, was inserted into the trachea. The cannula was then secured with silk suture thread (3-0 Ethicon, Johnson-Johnson, Belgium) passed through the holes of its plastic "butterfly." The cannula was then connected to a ventilation pump (Inspira ASV, Harvard Apparatus) and anesthetic gas delivery switched from the mask to the pump. Ventilation parameters were 70 bpm and tidal volume (Vt) in the range of 5.3–5.9 ml/kg. Starting Vt was chosen on the basis of measurements performed on a separate group of wild-type mice (n = 10).

Femoral Artery Cannulation
Femoral artery cannulation was performed at an IF level of 3%. We chose to cannulate the femoral artery instead of the femoral vein as customary in rat surgery due to the former's higher elasticity and resistance. This procedure allowed for quicker surgery and higher throughput compared to vein cannulation. The left leg of the animal was extended and taped on the surgical mat. A skin incision of roughly one centimeter was made above the femoral area. The left femoral artery was isolated and cannulated with a polyethylene catheter (PE10, OD 0.61 mm, ID 0.28 mm) filled with heparinized physiologic solution (25 UI/ml) containing 0.0375 mg/ml of pancuronium bromide that was continuously infused (rate 6.7 ml/kg/h) throughout the experiment to ensure constant neuromuscular blockade. This catheter was connected to a blood-pressure transducer (Biopac Systems) through a flow/flush device (CRITIFLO TA4004, Becton Dickinson). In order to allow for compound administration, a homemade Plexiglas Y-piece was placed in between the femoral catheter and the MABP transducer. The PE10 catheter was connected to the Y piece through a 2 cm PVC40 junction (OD 0.90 mm, ID 0.50 mm) inserted into a piece of Silicone tubing (Fr 3). The two-way system allowed simultaneous recording of MABP and infusion of paralyzing agent plus the injection of compounds (upon clamping of the opposite way to prevent the delivery of compound in the wrong line). After surgery (25–35 min in duration) mice

were placed into a customized stereotactic holder (Bruker, Germany) and anesthesia lowered to 1.2%.

rCBV Measurement

MRI data were acquired using a Bruker Avance 4.7 Tesla system, a 72 mm birdcage resonator for radiofrequency pulse transmit, and a Bruker curved "Mouse Brain" quadrature receive coil. The MR acquisition for each subject comprised T2-weighted anatomical images using the RARE sequence (Hennig et al., 1986; TR_{eff} = 5597 ms, TE_{eff} = 76 ms, RARE factor 8, FOV 40 mm, 256 × 256 matrix, 24 contiguous 0.75 mm slices) followed by a time series acquisition with the same spatial coverage and similar parameters (TR_{eff} = 5436 ms, TE_{eff} = 112 ms, RARE factor 32, 128 × 128 matrix, 24 contiguous 0.75 mm slices), but lower in-plane spatial resolution (312 μm^2) giving a functional pixel volume of ~0.07 mm^3. Two successive scans were averaged for a resulting time resolution of 42 s.

Total MRI time series acquisition time was 70 min (100 repetitions) for all groups. Following five reference images, 3.75 μl/g of the blood pool contrast agent Endorem (Guerbet, France) was injected so that subsequent signal changes would reflect alterations in relative cerebral blood volume (rCBV; Mandeville et al., 1998). The dose of Endorem was selected to ensure a mean signal decrease of ~60% necessary to optimize the contrast-to-noise ratio of the rCBV measurement as described (Mandeville et al., 1998). Each subject received an intra-arterial injection of vehicle (saline, 5 μl/g) followed by a challenge with 8-hydroxy-2-(di-n-propylamino) tetralin (8-OH-DPAT, Sigma, Milano) 25 min later. Vehicle injection was performed 15 min after administration of contrast agent. $Htr1a^{CeA}$ and wild-type littermates mice received anticholinergic agents (0.3 mg/kg, i.p.) or saline vehicle between intra-arterial vehicle and 8-OH-DPAT injections (14 min apart). The MRI time series were acquired over a period of 25 min following the administration of the 8-OH-DPAT challenge. The dose of 8-OH-DPAT and atropine were chosen based on previous in vivo studies (Tsetsenis et al., 2007; Gasbarri et al., 1997; Boccia et al., 2003; Baratti et al., 1979). Atropine sulfate is a nonselective acetylcholine muscarinic receptor antagonist; atropine methyl-nitrate is a non-brain-penetrant salt form of atropine. All compounds were injected at 1 ml/min. Compound injection was followed by administration of 0.2 ml of saline to flush the intra-arterial line.

fMRI Data Analysis

rCBV time series data for each experiment were analyzed within the framework of the general linear model (GLM) to obtain Z statistic maps (Worsley et al., 1992). Signal intensity changes in the time series were then converted into fractional rCBV changes on a pixel-wise basis using the transform (Mandeville et al., 1998) rCBV(t) = ln(S(t)/B(t))/ln(B(t)/SPRE), where S(t) is the measured signal, B(t) the estimated background signal in the absence of transient functional stimuli, and SPRE the signal intensity prior to administration of the contrast agent. B(t) was set equal to the mean signal intensity B_0 during the 8.4 min (12 time points) period prior to compound injection. For each time series, a rCBV time series surrounding the vehicle and 8-OH-DPAT injection points were calculated independently using identical parameters, covering 8.4 min (12 time points) prechallenge baseline and 22.4 min (32 time points) postchallenge window, normalized to a common injection time point. In contrast to what we observed in the rat (Schwarz et al., 2003) the slow rate of blood-pool contrast agent elimination from mouse blood resulted in negligible signal drifts over the time-window examined, which did not require the application of detrending corrections. The T_2-weighted anatomical images from each subject were coregistered by rigid body alignment to a brain template using FLIRT, Version 5.63, part of FSL (FMRIB's Software Library, www.fmrib.ox.ac.uk/fsl) and applying the resulting transformation matrix to the accompanying rCBV time series.

Two separate anatomical templates were created in order to account for the presence of slight but significant differences in the size of the brain of the transgenic lines (KO, CeA, and DG) with respect to wild-types, with the latter showing a reduced dorsoventral and horizontal extension. Average brain templates were created by coregistering and overlaying all the anatomical scans to a representative subjects using FSL/FLIRT (affine transformation, 6 degrees of freedom). Non-brain tissue was removed from the template using FSL/BET (brain extraction tool) followed by manual removal of residual signal

from spurious subcutaneous fat in posterior slices. The template thus obtained (template 1) was then used to mask individual anatomical images. The final template was created through a second iteration of the coregistration process using individual masked anatomicals and masked template 1 (affine, 7 degrees of freedom, FSL/FLIRT). The resulting transformation matrix was applied to the accompanying rCBV time series. The use of the paralyzing agent ensured that no motion-related effects were present in the time series. Data from all animals were checked for motion following acquisition by subtraction of image frames at beginning and end of the time series, and at intermediate points (e.g., before and after injection) revealing no motion artifacts in all the subjects examined.

Data were analyzed as previously described (Schwarz et al., 2006, 2007b). In brief, subjects were coregistered by rigid body alignment to a mouse brain template using FLIRT, Version 5.63, part of FSL (www.fmrib.ox.ac.uk/fsl). The template was created by coregistering and overlaying all the anatomical scans onto a representative subject using FSL/FLIRT. Signal time course analysis in pericranial ROIs of individual animals did not highlight significant motion artifacts in any of the subjects imaged. Signal intensity changes were converted into fractional rCBV changes (Mandeville et al., 1998). rCBV time series before and after intra-arterial injections were calculated with 8 and 28 pre- and postchallenge time points, respectively. Ten and 18 time points pre- and postadministration were used for intra-peritoneal administration. Activation/deactivation maps were analyzed using FEAT Version 5.63, part of FSL, with 0.8 mm spatial smoothing and model functions identified by Wavelet Cluster Analysis (Schwarz et al., 2006). Two separate regressors were identified for wild-type and $Htr1a^{CeA}$ subjects (Reg 1 and Reg 2, Figure S5). Image analysis of $Htr1a^{DG}$ and $Htr1a^{KO}$ was performed using Reg 1 as no plausible regressor describing 8-OH-DPAT was found. Group comparisons were carried out using FLAME (FMRIB's Local Analysis of Mixed Effects). Z (Gaussianised T/F) statistic images were thresholded using clusters determined by Z > 1.96 (unless otherwise described) and a corrected cluster significance threshold of p = 0.01 (Friston et al., 1994; Worsley et al., 1992). rCBV time series for 8-OH-DPAT, vehicle, or atropine injections (Figures S1–S4) were extracted bilaterally for specific regions of interest (ROIs) anatomically defined based on a mouse stereotactic atlas (Paxinos and Franklin, 2003). The effect of atropine pretreatment on the agonist response was assessed using average rCBV over an 8–20 min postinjection time window and one-way ANOVA followed by Fisher LSD. Results are quoted and displayed as mean ± SEM unless otherwise indicated.

Unsmoothed rCBV time series for 8-OH-DPAT and vehicle injection in each subject were extracted for specific regions of interest (ROIs) based on correspondence between the anatomical images and stereotactic atlas of the mouse brain (Paxinos and Franklin, 2003) using custom in-house software written in IDL (Research Systems, Boulder, CO). rCBV time course data were shown as group mean ± standard error (SEM). Regions examined (and their approximate rostrocaudal position from z_{bregma}) were amygdala (−1.58 mm), caudate putamen (+0.74 mm), ventral dentate gyrus (−4.24 mm), dorsal dentate gyrus (−1.34 mm), posterior dentate gyrus (−3.16 mm), thalamus (−1.82 mm), hypothalamus (−1.82 mm), motor cortex (+0.62 mm), somatosensory cortex (+0.02 mm), prefrontal cortex (+1.54 mm), and cingulate cortex (+0.74 mm). All ROIs were drawn bilaterally. Maps of correlated responses across subjects (Figure 3) were calculated within a General Linear Model framework at the higher level using FSL with FLAME as previously described (Schwarz et al., 2007b). Two reference (seed) regions, left CeA (z_{bregma} −0.6 mm) and left somatosensory cortex (z_{bregma} −0.9 mm), were selected a priori. Maps were thresholded using clusters determined by Z > 1.6 and a corrected cluster significance threshold of p = 0.01. Mean arterial blood pressure data were rebinned in 10 sample subdivisions and plotted using 40 s bins (Figure S6).

Arterial blood pressure time courses were recorded using an intra-arterial transducer and a 50 Hz sampling frequency (AcqKnowledge 3.1, Biopac Systems, Goleta). Mean arterial blood pressure (MABP) was calculated by temporally smoothing raw blood pressure traces using a moving average of 300 samples (6 s). MABP data were then rebinned in 10 subdivisions. Average MABP response over a 0–20 min postinjection time window was used as a summary measurement for statistical comparison between groups. Statistical comparison of MABP and arterial blood gases (p_aCO_2 and p_aO_2) was performed using one-way ANOVA followed by Fisher's LSD (least significant

difference) test using Statistica 8.0 (Statsoft, Tulsa, OK). To simplify data presentation, MABP time course data were plotted using 40 s bins.

The composition of the experimental groups and treatments is summarized as follows: Group 1 – $Htr1a^{KO}$, vehicle/8-OH-DPAT, n = 8; Group 2 – $Htr1a^{CeA}$, vehicle/vehicle/8-OH-DPAT, n = 9; Group 3 – $Htr1a^{CeA}$, vehicle/atropine-sulfate/8-OH-DPAT, n = 5; Group 4 – $Htr1a^{CeA}$, vehicle/atropine-methyl-nitrate/8-OHDPAT, n = 5; Group 5 – $Htr1a^{DG}$, vehicle/8-OH-DPAT, n = 6; Group 6 – wild-type, vehicle/8-OH-DPAT, n = 14; Group 7 – wild-type vehicle/vehicle/8-OH-DPAT, n = 8; Group 8 – wild-type, vehicle/atropine-sulfate/8-OH-DPAT, n = 8.

Immunohistochemistry

Undisturbed littermates were injected with 8-OH-DPAT (one mouse/genotype/cage) and returned to their home cage for 90 min before trans-cardial perfusion with saline and paraformaldehyde under anesthesia. Brains were removed, postfixed overnight, and rapidly frozen before cryosectioning (40 μm). Anti-c-Fos (Calbiochem) immunohistochemistry was carried out on free-floating coronal brain sections using the ABC detection system (Vector Labs). Immunostaining was quantified manually from microscope images of matched sections (two sections/animal; averaging between hemispheres) with the aid of Image J software.

Behavioral Testing

Fear conditioning was carried out as previously described (Tsetsenis et al., 2007). In brief, mice were exposed on day 1 to a partially conditioned tone and a perfectly conditioned light stimulus (20 s stimulus coterminating with 0.5 mA, 1 s footshock, 3× tone-light-shock, 2× tone interspersed; tone: 3000 Hz, 85 dB), and tested for freezing during the tone delivered in a novel cage on day 2 (3 min baseline period followed by 6 min tone presentation). Behavioral data were extracted by manual scoring of video recordings from the 3 min baseline and first 3 min of the tone presentation with the aid of Observer software (Noldus, Wageningen, Netherlands). Digging was scored when the animal was close to the edge of the cage and was using his paws to dig and pull up the plastic flooring. Exploration was scored when the animal made pronounced whole-body movements that extended across the cage. Rearing included both wall and center rearing. All behaviors were recorded as total duration of the activity. All scoring was performed blind to genotype and treatment.

Electrophysiological Recordings

Mice (P21-P55 littermates) were deeply anesthetized with halothane and decapitated, and whole brains were rapidly removed and immersed for 10 min in oxygenated (95% O_2, 5% CO_2 [pH 7.4]) ice-cold ACSF containing 125 mM NaCl, 2.5 mM KCl, 1.25 mM NaH_2PO_4, 1.0 mM $MgCl_2$, 2.0 mM $CaCl_2$, 10 mM glucose, and 26 mM $NaHCO_3$. Horizontal (250 μm) slices were cut at 4°C with a vibratome, placed in a chamber containing oxygenated ACSF, and allowed to recover for 2 hr at room temperature. Individual slices were then transferred to the submerged slice-recording chamber and maintained at 32°C and constantly superfused with oxygenated ACSF. Central amygdala regions were identified using the hippocampus CA2 and lateral amygdala regions as references. Recording electrode resistance was 8–12 MΩ when filled with an intracellular solution of 140 mM K-gluconate, 4 mM $MgCl_2$, 0.5 mM EGTA, 10 mM HEPES, 2 mM MgATP, and 0.5 mM NaGTP (pH 7.3, 280 mOsm). Whole-cell recordings were made using an amplifier (Multiclamp 700B, Axon Instruments) and signals filtered and digitized at 10 kHz with an A/D converter (Digidata 1322A, Axon Instruments) and stored using pClamp 9 software (Axon Instruments). Spontaneous firing was recorded in current-clamp configuration with neurons held near the spiking threshold (−55 ± 5mV) by depolarizing current injection. In some experiments spontaneous frequency was enhanced by lowering ACSF Ca^{2+} concentration to 0.5 mM. Baseline activity was monitored for at least 4 min and stable baseline spiking frequency obtained before applying agonists. Drugs were freshly prepared from stock solutions and applied to the slice by a gravity-driven perfusion system (flow rate = 2 ml/min, one exchange every 3 min). Washout of agonists with ACSF reestablished spiking to initial levels within 10–15 min. Spontaneous spiking activity was analyzed by Mini Analysis Program (Synaptosoft, Decatur, GA) with detection parameters adjusted for each

data file to obtain correct values of peak amplitude and frequency both in simple events and complex bursts. Mean spike frequency time course was obtained by averaging the interevent interval in 10 s bins. Effects of drugs application were quantified by averaging spike frequency at baseline and the effect plateau (1–2 min each).

Statistical Testing

Statistical testing of behavioral data was carried out using ANOVA and Fisher LSD post-hoc testing in cases of significance, except for the atropine study in which we tested the a priori hypothesis that atropine would reverse the behavioral effects of 8-OH-DPAT and used t tests. c-Fos and electrophysiological data were analyzed by t test. Correlation was assessed by Pearson's regression testing. Statistical testing of imaging data is described above or in the figure legends.

SUPPLEMENTAL INFORMATION

Supplemental Information includes six figures and one table and can be found online at doi:10.1016/j.neuron.2010.07.008.

REFERENCES

Aggleton, J.P. (1992). The Amygdala (New York: Wiley-Liss).

Amaral, D., Price, J., Pitkanen, A., and Carmichael, T. (1992). Anatomical organization of the primate amygdaloid complex. In The Amygdala: Neurobiological Aspects of Emotion, Memory, and Mental Dysfuncton, J.P. Aggleton, ed. (New York: Wiley-Liss), pp. 1–66.

Baratti, C.M., Huygens, P., Mino, J., Merlo, A., and Gardella, J. (1979). Memory facilitation with posttrial injection of oxotremorine and physostigmine in mice. Psychopharmacology (Berl.) 64, 85–88.

Boccia, M.M., Blake, M.G., Acosta, G.B., and Baratti, C.M. (2003). Atropine, an anticholinergic drug, impairs memory retrieval of a high consolidated avoidance response in mice. Neurosci. Lett. 345, 97–100.

Cezario, A.F., Ribeiro-Barbosa, E.R., Baldo, M.V.C., and Canteras, N.S. (2008). Hypothalamic sites responding to predator threats—the role of the dorsal premammillary nucleus in unconditioned and conditioned antipredatory defensive behavior. Eur. J. Neurosci. 28, 1003–1015.

Chen, Y.-C.I., Mandeville, J.B., Nguyen, T.V., Talele, A., Cavagna, F., and Jenkins, B.G. (2001). Improved mapping of pharmacologically induced neuronal activation using the IRON technique with superparamagnetic blood pool agents. J. Magn. Reson. Imaging 14, 517–524.

Davis, M., and Whalen, P.J. (2001). The amygdala: vigilance and emotion. Mol. Psychiatry 6, 13–34.

Dringenberg, H.C., and Vanderwolf, C.H. (1997). Neocortical activation: modulation by multiple pathways acting on central cholinergic and serotonergic systems. Exp. Brain Res. 116, 160–174.

Ehrlich, I., Humeau, Y., Grenier, F., Ciocchi, S., Herry, C., and Lüthi, A. (2009). Amygdala inhibitory circuits and the control of fear memory. Neuron 62, 757–771.

Ferrari, L., Crestan, V., Sabattini, G., Vinco, F., Fontana, S., and Gozzi, A. (2010). Brain penetration of local anaesthetics in the rat: implications for experimental neuroscience. J. Neurosci. Methods 186, 143–149.

Friston, K.J., Jezzard, P., and Turner, R. (1994). Analysis of functional MRI time-series. Hum. Brain Mapp. 1, 153–171.

Gasbarri, A., Sulli, A., Pacitti, C., Puglisi-Allegra, S., Cabib, S., Castellano, C., Introini-Collison, I., and McGaugh, J.L. (1997). Strain-dependent effects of D2 dopaminergic and muscarinic-cholinergic agonists and antagonists on memory consolidation processes in mice. Behav. Brain Res. 86, 97–104.

Gozzi, A., Ceolin, L., Schwarz, A., Reese, T., Bertani, S., and Bifone, A. (2007). A multimodality investigation of cerebral haemodynamics and autoregulation in phMRI. Magn. Reson. Imaging 25, 826–833.

Hennig, J., Nauerth, A., and Friedburg, H. (1986). RARE imaging: a fast imaging method for clinical MR. Magn. Reson. Med. 3, 823–833.

Huber, D., Veinante, P., and Stoop, R. (2005). Vasopressin and oxytocin excite distinct neuronal populations in the central amygdala. Science 308, 245–248.

Jenkins, B.G., Chen, Y.-C.I., and Mandeville, J.B. (2003). Pharmacological magnetic resonance imaging (phMRI). In Biomedical Imaging in Experimental Neuroscience, N. van Bruggen and T. Roberts, eds. (New York: CRC Press), pp. 155–209.

Jolkkonen, E., Miettinen, R., Pikkarainen, M., and Pitkänen, A. (2002). Projections from the amygdaloid complex to the magnocellular cholinergic basal forebrain in rat. Neuroscience 111, 133–149.

LeDoux, J.E. (2000). Emotion circuits in the brain. Annu. Rev. Neurosci. 23, 155–184.

Lopez De Armentia, M., and Sah, P. (2004). Firing properties and connectivity of neurons in the rat lateral central nucleus of the amygdala. J. Neurophysiol. 92, 1285–1294.

Luo, L., Callaway, E.M., and Svoboda, K. (2008). Genetic dissection of neural circuits. Neuron 57, 634–660.

Luscher, C., Jan, L.Y., Stoffel, M., Malenka, R.C., and Nicoll, R.A. (1997). G protein-coupled inwardly rectifying K+ channels (GIRKs) mediate postsynaptic but not presynaptic transmitter actions in hippocampal neurons. Neuron 19, 687–695.

Mandeville, J.B., Marota, J.J.A., Kosofsky, B.E., Keltner, J.R., Weissleder, R., Rosen, B., and Weisskoff, R. (1998). Dynamic functional imaging of relative cerebral blood volume during rat forepaw stimulation. Magn. Reson. Med. 39, 615–624.

Mesulam, M.M., Mufson, E.J., Wainer, B.H., and Levey, A.I. (1983). Central cholinergic pathways in the rat: an overview based on an alternative nomenclature (Ch1-Ch6). Neuroscience 10, 1185–1201.

Paxinos, G., and Franklin, K. (2003). The Mouse Brain in Stereotaxic Coordinates (Sydney: Academic Press).

Roozendaal, B., Schoorlemmer, G.H., Wiersma, A., Sluyter, S., Driscoll, P., Koolhaas, J.M., and Bohus, B. (1992). Opposite effects of central amygdaloid vasopressin and oxytocin on the regulation of conditioned stress responses in male rats. Ann. N.Y. Acad. Sci. 652, 460–461.

Sah, P., Faber, E.S.L., Lopez De Armentia, M., and Power, J. (2003). The amygdaloid complex: anatomy and physiology. Physiol. Rev. 83, 803–834.

Schiess, M.C., Callahan, P.M., and Zheng, H. (1999). Characterization of the electrophysiological and morphological properties of rat central amygdala neurons in vitro. J. Neurosci. Res. 58, 663–673.

Schwarz, A.J., Reese, T., Gozzi, A., and Bifone, A. (2003). Functional MRI using intravascular contrast agents: detrending of the relative cerebrovascular (rCBV) time course. Magn. Reson. Imaging 21, 1191–1200.

Schwarz, A.J., Whitcher, B., Gozzi, A., Reese, T., and Bifone, A. (2006). Study-level wavelet cluster analysis and data-driven signal models in pharmacological MRI. J. Neurosci. Methods 159, 346–360.

Schwarz, A.J., Gozzi, A., Reese, T., and Bifone, A. (2007a). Functional connectivity in the pharmacologically activated brain: resolving networks of correlated responses to d-amphetamine. Magn. Reson. Med. 57, 704–713.

Schwarz, A.J., Gozzi, A., Reese, T., and Bifone, A. (2007b). In vivo mapping of functional connectivity in neurotransmitter systems using pharmacological MRI. Neuroimage 34, 1627–1636.

Sheth, S.A., Nemoto, M., Guiou, M., Walker, M., Pouratian, N., Hageman, N., and Toga, A.W. (2004). Columnar specificity of microvascular oxygenation and volume responses: implications for functional brain mapping. J. Neurosci. 24, 634–641.

Swanson, L.W., and Petrovich, G.D. (1998). What is the amygdala? Trends Neurosci. 21, 323–331.

Tribollet, E., Barberis, C., Jard, S., Dubois-Dauphin, M., and Dreifuss, J.J. (1988). Localization and pharmacological characterization of high affinity binding sites for vasopressin and oxytocin in the rat brain by light microscopic autoradiography. Brain Res. 442, 105–118.

Tsetsenis, T., Ma, X.H., Lo Iacono, L., Beck, S.G., and Gross, C. (2007). Suppression of conditioning to ambiguous cues by pharmacogenetic inhibition of the dentate gyrus. Nat. Neurosci. 10, 896–902.

Veinante, P., and Freund-Mercier, M.J. (1997). Distribution of oxytocin- and vasopressin-binding sites in the rat extended amygdala: a histoautoradiographic study. J. Comp. Neurol. 383, 305–325.

Viviani, D., and Stoop, R. (2008). Opposite effects of oxytocin and vasopressin on the emotional expression of the fear response. Prog. Brain Res. 170, 207–218.

Walker, D.L., and Davis, M. (2008). Role of the extended amygdala in short-duration versus sustained fear: a tribute to Dr. Lennart Heimer. Brain Struct. Funct. 213, 29–42.

Wilensky, A.E., Schafe, G.E., Kristensen, M.P., and LeDoux, J.E. (2006). Rethinking the fear circuit: the central nucleus of the amygdala is required for the acquisition, consolidation, and expression of Pavlovian fear conditioning. J. Neurosci. 26, 12387–12396.

Worsley, K.J., Evans, A.C., Marrett, S., and Neelin, P. (1992). A three-dimensional statistical analysis for CBF activation studies in human brain. J. Cereb. Blood Flow Metab. 12, 900–918.